



Effect of Ti(IV) loading on CH₄ oxidation activity and SO₂ tolerance of Pd catalysts supported on silica SBA-15 and HMS

A.M. Venezia^{a,*}, G. Di Carlo^b, L.F. Liotta^a, G. Pantaleo^a, M. Kantcheva^c

^a Istituto per lo Studio dei Materiali Nanostrutturati (ISMN-CNR), via Ugo La Malfa, 153, Palermo I- 90146, Italy

^b Istituto per lo Studio dei Materiali Nanostrutturati (ISMN-CNR), via Salaria km 29300, 00015 Monterotondo Stazione, Rome, Italy

^c Department of Chemistry, Bilkent University, 06800 Bilkent, Ankara, Turkey

ARTICLE INFO

Article history:

Received 4 April 2011

Received in revised form 3 June 2011

Accepted 11 June 2011

Available online 17 June 2011

Keywords:

Pd catalyst
CH₄ oxidation
TiO₂-SBA-15
TiO₂-HMS
SO₂ effect

ABSTRACT

Pure silica SBA-15 and HMS and corresponding Ti(IV) modified mesoporous silica, with 5 and 10 wt% of TiO₂, were prepared and used as support for palladium (1 wt%) catalysts. The materials, analysed by XPS, XRD, BET, NH₃-TPD and FT-IR techniques, were tested in the total oxidation of methane. The catalytic activity was measured in lean conditions at WHSV = 60,000 ml g⁻¹ h⁻¹ in the absence and presence of 10 vol. ppm SO₂. Moreover, the effect of a prolonged reaction aging and severe SO₂ poisoning on the catalytic performance of the best performing catalyst was investigated. The addition of TiO₂ improved the catalytic performance of the SBA-15 supported catalysts by increasing the sulfur tolerance and most importantly by favoring the regeneration of the catalyst in subsequent SO₂-free runs. An opposite behavior was observed with the palladium supported on Ti(IV)-modified HMS support which exhibited lower activity and a substantial worsening of the SO₂ tolerance as compared to palladium supported on pure HMS. On the bases of the structural and chemical investigation, the differences between the two series of catalysts were ascribed to the distinct structural and acidic properties of the supports. In particular, the good performance of the Ti(IV) doped SBA-15 supported catalysts was due to the combination of Ti(IV) structurally incorporated into the silica lattice and present as surface dispersed TiO₂ particles. The negative effect of the Ti(IV) over the HMS supported catalysts was related to the high acidity induced by the more homogeneous incorporation of Ti(IV) into the silica structure.

© 2011 Elsevier B.V. All rights reserved.

1. Introduction

Natural gas, mainly consisting of methane, is increasingly replacing gasoline or diesel as fuel for transportation vehicles [1,2]. The reason for this change is the decline of the petroleum reserves and the lower emission of pollutants associated with the combustion of methane. Since the natural gas fuelled vehicles (NGV) typically run at low temperature (320–420 °C) the emission of NO_x is lower and due to the high H:C ratio also the produced CO₂ is less as compared to the other fuel driven vehicles [2]. Nevertheless a major concern related to the use of natural gas is the emission of the unburned methane which has an even stronger greenhouse effect as compared to the CO₂ [3]. Since methane is an almost inert molecule, it requires high temperature for its complete oxidation. A crucial step in the achievement of the total combustion process is the activation of the first C–H bond [4,5]. Either homolytic bond cleavage with the formation of radicals, or heterolytic C–H bond cleavage at the acid–base pair of sites is generally considered. In any case, in order to increase the efficiency of the methane com-

bustion at low temperature (below 600 °C) it is necessary to use a suitable catalyst. For this specific reaction, two classes of catalysts are currently investigated, those based on transition metal oxides as solid solution oxides [6,7], perovskites [8,9], hexaaluminate [10], and those based on noble metals [11–14]. Among this latter class, Pd-based catalysts are the most active for the methane total oxidation at low temperatures. As pointed out in several studies, their catalytic activity depends strongly on the nature of the support [12], on the palladium precursors [15,16] and on the size of the PdO particles [17]. Their major drawback is represented by their easy poisoning by sulfur derived from the gas and engine lubricating oil [11]. According to the literature, when a sulfating support like Al₂O₃ is used, palladium deactivates slowly, due to the preferential interaction of SO_x with the support, at variance with palladium over the inert SiO₂ deactivating quickly because of the direct interaction between palladium and SO_x. Nevertheless, the use of silica, in the absence of particle sintering, allows an easier regeneration of the sulfur-poisoned catalyst through the thermal decomposition of the palladium sulfate occurring at temperature above 600 °C [1,11]. Recent studies in our group have shown that both methane conversion activity and sulfur tolerance could be improved substantially by using high surface area silica with specific characteristic of acidity and morphology. In particular, supporting palladium on

* Corresponding author. Tel.: +39 0916809372; fax: +39 0916809399.
E-mail addresses: venezia@pa.ismn.cnr.it, anna@pa.ismn.cnr.it (A.M. Venezia).

mesoporous silica HMS yielded more efficient and more sulfur resistant catalysts as compared to a lower surface area silica supported catalyst [18]. Incorporation of a precise amount (10 wt%) of TiO_2 during the sol–gel preparation of amorphous silica produced an additional improvement of the sulfur tolerance during the methane oxidation in the presence of SO_2 , still allowing the complete catalyst regeneration typical of a silica support [19,20]. The positive behavior was attributed to the combination of the high surface area support and the scavenger action of the sulfating oxide like TiO_2 . Within this frame, the present study intends to further improve the catalytic behavior of palladium for the oxidation of methane by using titania-doped silica mesoporous materials as catalyst supports. To this aim two series of palladium catalysts supported on Ti(IV)-modified HMS and Ti(IV)-modified SBA-15 were prepared. In order to compare with the previous sol–gel prepared titania modified silica [19], Ti(IV) was incorporated using the one step synthesis in which titanium precursor was added during the preparation of the mesoporous materials. To evaluate the effect of the support structure on the Pd activity and stability, analyses by XPS, XRD, BET, NH_3 -TPD and FT-IR techniques were performed.

2. Experimental

2.1. Support and catalyst preparation

The mesostructured HMS material was synthesized according to a published procedure [21]. Basically, HMS was assembled from 4:1 molar mixtures of tetraethyl orthosilicate (TEOS) (Aldrich) as the inorganic precursor and dodecylamine (DDA) (Aldrich) as the structure-directing surfactant in 90:10 (v/v) water/ethanol. About 49 mmol of DDA were dissolved in 50 ml of ethanol and 450 ml of H_2O . To the surfactant solution, heated to 60°C , 196 mmol of TEOS were added. The gel mixture was kept in a closed Teflon vessel at 60°C for 20 h. The reaction product was filtered, washed with distilled water and dried at room temperature for 24 h. The surfactant was removed by calcination in air at 500°C for 4 h. Titanium containing HMS materials were synthesized according to the procedure reported by Tanev et al. [22] using $\text{Ti}(\text{iso-OC}_3\text{H}_7)_4$ (Aldrich) as titanium precursor, and following the same steps as above. The titanium precursor was added in appropriate amount to yield a 5 wt% and 10 wt% of TiO_2 in the final mixed oxide.

SBA-15 was synthesized following a procedure described by Zhao et al. [23]. Accordingly, 8.1 g of Pluronic P123 (EO20PO70EO20, Aldrich) was dissolved in 146.8 g distilled water and 4.4 g of conc. HCl (37%) and stirred over night at 35°C . To this solution 16 g of TEOS ($\text{Si}(\text{OC}_2\text{H}_5)_4$, Aldrich 98%) was quickly added and stirred for 24 h at 35°C . The suspension was annealed at 100°C for 24 h in closed polypropylene bottle. The solid product was filtered, washed with water and calcined at 500°C for 5 h in air. Similar procedure was used for the synthesis of the titanium containing SBA-15 materials. The main difference consisted in the pre-hydrolysis of TEOS for 5 h at 35°C before adding appropriate amount of $\text{Ti}(\text{iso-OC}_3\text{H}_7)_4$ drop by drop under vigorous stirring. The titanium precursor was added in appropriate amount to yield samples with 5 wt% and 10 wt% of TiO_2 in the final oxide.

Attainment of the ordered mesoporous structures was confirmed by the SAXS patterns and by the typical type IV N_2 adsorption–desorption isotherms [21,24].

Palladium was deposited by wet impregnation using an aqueous solution of palladium nitrate in the appropriate amount to yield 1 wt% Pd loaded catalysts. The samples were calcined at 500°C for 4 h. The chemical composition of the samples was checked by X-ray fluorescence analyses. The samples were labelled Pd/HMS, Pd/Ti_xHMS, Pd/SBA-15 and Pd/Ti_xSBA-15 where x represented the TiO_2 weight percentage (wt%).

2.2. Catalyst characterization

X-ray diffraction patterns were measured with a Philips vertical goniometer using Ni-filtered $\text{Cu K}\alpha$ radiation. A proportional counter and 0.05° step sizes in 2θ were used. The assignment of the various crystalline phases was based on the JPDFS powder diffraction file cards [25]. From the line broadening of the main reflection peaks, using the Scherrer equation, particle sizes above the detection limits of 3 nm were determined [26].

SAXS measurements were performed with BRUKER AXS NANOSTAR with step sizes of 0.02° in 2θ .

X-ray fluorescence was performed using the Bruker S2 Ranger spectrophotometer.

The microstructural properties of the materials were determined from N_2 adsorption–desorption isotherms at -196°C using a Sorptomatic 1900 (Carlo Erba) instrument. Before the measurements, samples were heated in vacuum at 250°C for 2 h. Specific surface areas and pore distributions of the materials were obtained respectively using the Brunauer–Emmett–Teller (BET) and the Barret–Joyner–Hatenda (BJH) calculation methods [24].

The X-ray photoelectron spectroscopy analyses were performed with a VG Microtech ESCA 3000 Multilab, using the unmonochromatized $\text{Al K}\alpha$ source (1486.6 eV) run at 14 kV and 15 mA. For the individual peak energy regions, a pass energy of 20 eV was used. Samples were mounted with double-sided adhesive tape. Binding energies were referenced to the C 1s binding energy of adventitious carbon set at 285.1 eV. The software provided by VG was used for peak analyses and for the calculation of the atomic concentrations. The precision on the binding energy and on the atomic percentage values was respectively ± 0.15 eV and $\pm 10\%$.

The acidity of the oxide catalysts was determined by measurements of temperature-programmed desorption of ammonia (NH_3 -TPD). The sample amount of 0.1 g was out-gassed in a 5 vol.% O_2/He flow at 500°C for 1 h. This was followed by ammonia-saturation by flowing 5% NH_3/He stream (30 ml/min) at room temperature for 1 h. After purging with 100 ml/min He flow for 1 h at 100°C and then cooling down to room temperature, the catalyst was heated under He (30 ml/min) in a linear rate of $10^\circ\text{C}/\text{min}$ to 950°C and the ammonia desorption was continuously monitored by the TCD. In order to determine the total acidity of the catalyst from its NH_3 desorption profile, the area under the curve was integrated.

The type of acidity (Lewis and Brønsted) was investigated by FT-IR spectroscopy of adsorbed pyridine. The FT-IR spectra were recorded using a Bomem Hartman & Braun MB-102 model FT-IR spectrometer with a liquid-nitrogen cooled MCT detector at a resolution of 4 cm^{-1} (100 scans). The self-supporting discs ($\sim 0.013\text{ g}/\text{cm}^2$) were activated in the IR cell by heating for 1 h in a vacuum at 450°C and in oxygen (100 mbar, passed through a trap, cooled in liquid nitrogen) at the same temperature, followed by evacuation for 1 h at 450°C . The pyridine (Sigma–Aldrich) adsorption test was carried out by the admission of 1.6 mbar of the base into the IR cell, left in contact with the sample for 15 min. The excess pyridine was then evacuated at room temperature for 15 min, followed by a desorption of the strongly bonded base fraction in the temperature range 25 – 250°C . The spectra of the adsorbed compounds were obtained by subtracting the spectra of the activated samples from the spectra recorded. The sample spectra were also gas-phase corrected.

2.3. Catalytic activity

Methane oxidation catalytic tests were performed using a U shaped quartz reactor with an inner diameter of 12 mm, electrically heated in a furnace. The catalyst powder (sieved fraction between 180 and $250\ \mu\text{m}$) was diluted 1:2 with inert SiC, in order to avoid

thermal gradients, and it was placed on a porous quartz disk. The reaction temperature was measured by a K-type thermocouple in contact with the catalytic bed long 12 mm. Prior to the catalytic testing, the samples were treated “in situ” under flowing O₂ (5 vol.% in He, 50 ml/min) at 350 °C for 0.5 h and under He during cooling at 200 °C. The standard reagent gas mixture, consisting of 0.3 vol.% of CH₄ + 2.4 vol.% O₂ in He, was led over the catalyst (50 mg) at a flow rate of 50 ml/min (STP), equivalent to a weight hourly space velocity (WHSV) of 60,000 ml g⁻¹ h⁻¹. Activities were measured by increasing the temperature from 200 °C to 600 °C (by steps of 50 °C, hold time 45 min). The inlet and outlet gas compositions were analysed by on line mass quadrupole (Thermostar™, Balzers), in order to follow the evolution of all the species, CH₄, CO, CO₂, H₂, H₂O, O₂. Moreover, the concentrations of CO, CO₂ and CH₄ species were checked by IR analysers (ABB Uras 14, Uras 26), calibrated in the range 0–3000 ppm for CO, 0–10,000 ppm for CO₂ and 0–30,000 ppm for CH₄. The reaction products of methane oxidation were CO₂ and H₂O. No CO was detected in the overall range of temperature. Carbon balance was close to ±5% in all the catalytic tests. Experiments of methane oxidation in the presence of SO₂ were performed by co-feeding 10 vol. ppm of SO₂. Between consecutive runs the sample was cooled down in He atmosphere.

3. Results and discussion

3.1. Characterization

3.1.1. N₂ adsorption–desorption analyses

The N₂ adsorption and desorption isotherms of the pure silica supports and of the titania doped ones are shown in Fig. 1. The

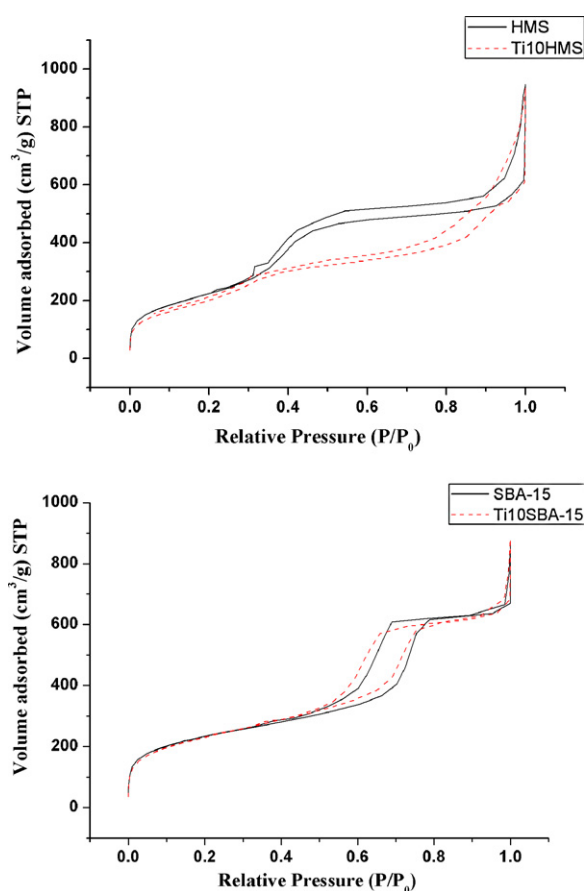


Fig. 1. Nitrogen adsorption–desorption isotherms of pure and Ti(IV) doped HMS and SBA-15 supports.

Table 1

Textural and structural data of pure and Ti(IV)-modified SBA-15 and HMS supports.

Sample	S_a (m ² /g)	d_p ^b (nm)	V_p ^c (cm ³ /g)	a_0 ^d	d_w ^e (nm)
HMS	824	3.2	0.99	4.6	1.4
Ti5HMS	845	2.5	1.33	4.5	2.0
Ti10HMS	728	2.6	1.00	4.3	1.7
SBA-15	838	7.7	0.99	11.3	3.6
Ti5SBA-15	912	7.1	1.35	11.3	4.2
Ti10SBA	841	7.1	0.96	11.0	3.9

^a The BET surface area values were calculated in the range 0.05–0.2p/p⁰.

^b The mean pore diameter determined using the BJH model from N₂ adsorption/desorption isotherms.

^c The pore volume determined considering the range p/p⁰ from 0.1 until to 0.98.

^d Unit cell parameter calculated as $a_0 = 2d_{100} \sqrt{3}$ with d_{100} being the plane distance computed according to the Bragg's law ($\lambda = 2d \sin \theta$). a_0 corresponds to the distance between the pores.

^e The wall thickness calculated as $d_w = a_0 - d_p$.

isotherms are of type IV, with hysteresis loops characteristic of mesoporous compounds. According to the IUPAC classification, the hysteresis loops of the SBA-15 and HMS can be classified as H1 and H3 types, respectively [24]. As already reported in literature, the hysteresis loops of the SBA-15 and Ti_xSBA-15 supports are larger and typically of the presence of mesopores [27]. In contrast, the hysteresis loops of HMS and Ti_xHMS are rather flat and extended over a large range of relative pressures, indicating the presence of both framework mesoporosity and interparticle macroporosity [27]. The textural properties are summarised in Table 1. The BET surface areas of the HMS and SBA-15 supports are similar and quite large. Both supports are slightly affected by the presence of titania. As a function of the titania loading the surface areas do not follow any clear trend, on the contrary, the pore diameters decrease. As expected, the average pore diameters of the SBA-15 series are more than double those of the HMS series.

3.1.2. SAXS

The SAXS patterns of the two series of supports are shown in Fig. 2. The corresponding unit cell parameters (a_0), and the wall thickness (d_w) are provided in Table 1. The unit cell parameters were calculated as $a_0 = 2d_{100} \sqrt{3}$, assuming a hexagonal unit cell for both series of supports. The wall thickness was estimated by subtracting from a_0 the pore diameters obtained from the N₂ physisorption measurements. The SAXS curves of the HMS samples are characterized by one main broad peak, at around $2\theta \approx 2^\circ$ corresponding to a unit cell parameters of ≈ 4.4 nm attributed to a bi-dimensional hexagonal structure [21]. The insertion of titanium in HMS resulted in a progressive loss of this long-range order and in a slight decrease of the unit cell parameter. On the contrary SBA-15 exhibits three main reflection peaks indexed as (1 0 0), (1 1 0) and (2 0 0) typical of a more ordered material, with a unit cell parameter of ≈ 11.3 nm. The insertion of titania does not change significantly the original hexagonal structure but, in accord with the decreased peak intensity, slightly causes a deterioration of the long range order. As shown in Table 1, a slight decrease of the unit cell parameters is observed for the titania containing supports and correspondingly an increase of the framework wall thickness, to a large extent in the HMS series. This effect would confirm a certain degree of titania incorporation in the structure of the silica [28,29]. The

Table 2

Acid properties of the supports as determined by TPD-NH₃ in the range 50–500 °C.

Sample	T (°C)	V_{NH_3} (ml g ⁻¹)
HMS	114	1.4
Ti10HMS	157	7.8
SBA-15	118	2.0
Ti10SBA-15	126	2.9

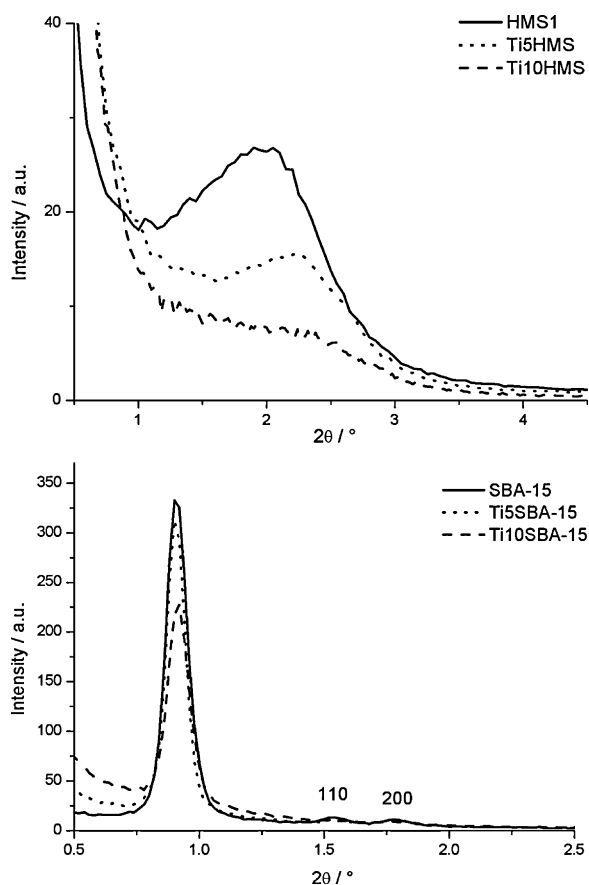


Fig. 2. SAXS Curves of pure and Ti(IV) doped HMS and SBA-15 supports.

subsequent impregnation of palladium leaves unchanged the SAXS patterns (not shown in here for brevity) of both series of supports.

3.1.3. TPD-NH₃

The change of acidity upon insertion of titania was investigated by temperature programmed desorption of ammonia. The technique provided information on the total acidity of the solids, including both Brønsted and Lewis acidity and accounting for the different strength and number of acid sites. The TPD patterns of the pure and of the 10 wt% TiO₂ doped mesoporous silicas are shown in Fig. 3. The results are summarised in Table 2, in terms of temperature of NH₃ desorption and volumes of desorbed NH₃. For both types of mesoporous materials only the first peak was considered. Indeed the other feature, consisting of a broad peak observed only in the SBA-15 samples, was due to the evolution of water and organic materials, as detected by the quadrupole measurements, and therefore not included in the acidity evaluation. According to the patterns and to the values listed in Table 2, it is evident that the insertion of Ti(IV) in HMS caused a substantial increase of acidity in terms of both, strength and number of acid sites. On the contrary the addition of titanium in SBA-15 produced only a limited acidity changes.

3.1.4. XRD analyses

In order to identify the crystalline phases present in the samples the X-ray diffraction analyses of the supported palladium catalysts were performed. In Fig. 4 the corresponding diffractograms are shown along with the diffraction lines of the reference phases, anatase TiO₂ and PdO. The XRD patterns show a broad diffraction band between 20° and 30° 2θ attributed to the amorphous part of the substrate. Characteristic PdO peaks are present in the patterns

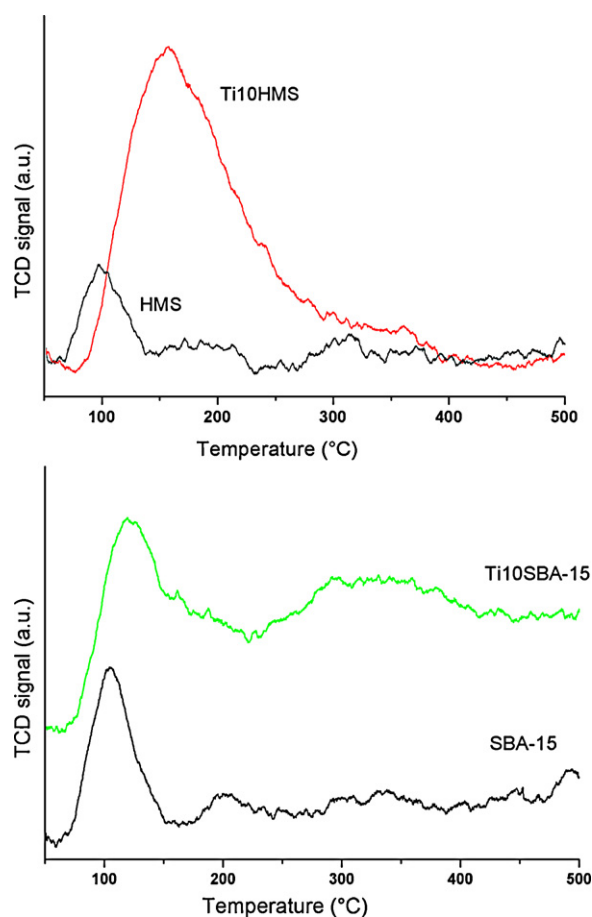


Fig. 3. TPD-NH₃ patterns in the range 50–500 °C of the mesoporous supports.

of both series of samples. The anatase phase is visible in the Ti(IV)-doped SBA-15 samples, but not in the Ti(IV)-doped HMS series. The anatase phase was also observed in a similarly prepared Ti-SBA-15 material containing 2.5 at% Ti. DRS UV-vis spectra of this sample presented an absorption band around 334 nm due to Ti⁴⁺ in octahedral coordination typical of the anatase [30]. Generally speaking, preparation of ion-doped SBA-15 by direct incorporation during the synthesis of the mesoporous oxide is rather difficult due to the strong acidic media [31]. Indeed, under strongly acidic conditions (pH < 1) free titanium species such as Ti⁴⁺ exist only in cationic form and thus are not able to enter the framework of SBA-15 [32]. The grafting procedure using several types of titanium precursors allows inserting only about 6 at% of titanium relative to silicon into SBA-15 matrix. Higher titania loadings, 8–10 at% as in the present case (used Si/Ti ratios of 25 and 12), would produce anatase crystallites of TiO₂ [33]. In the present work, the direct synthesis procedure adopted for the pure SBA-15 was intentionally used, aiming to investigate the effect of TiO₂ either formed as aggregates and also as structural modifier. By applying the Scherrer equation to the line width of the main reflection peaks, the diameters of the PdO and TiO₂ particles in the different samples were estimated. The corresponding calculated values are listed in Table 3. TiO₂ particle size of 8 nm were obtained for the SBA-15 supported catalysts, whereas PdO particle sizes of 6–7 nm were obtained for all the samples, included also the HMS supported ones.

3.1.5. XPS analyses

Information on the chemical state and the surface chemical composition of the palladium samples, before the catalytic tests, were obtained by XPS analyses. In Table 4 the Pd 3d_{5/2}, the Ti

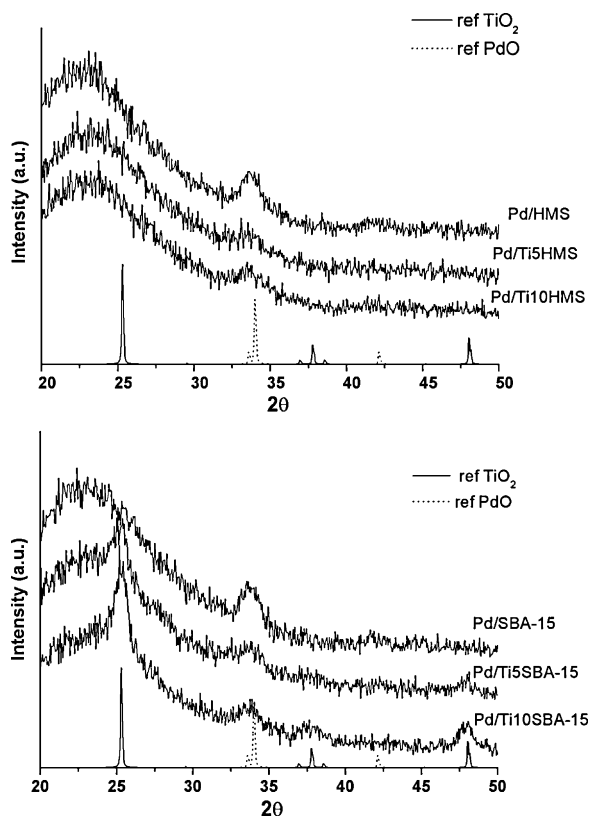


Fig. 4. XRD patterns of SBA-15 and HMS supported palladium catalysts with and without Ti(IV). The patterns of pure anatase TiO₂ and PdO oxides are shown as references.

Table 3
XRD derived PdO and TiO₂ particle diameters in the fresh samples.

Sample	d_{PdO} (nm)	d_{TiO_2} (nm)
Pd/SBA-15	6	–
Pd/Ti5SBA-15	6	8
Pd/Ti10SBA-15	7	8
Pd/HMS	7	–
Pd/Ti5HMS	6	n.d. ^a
Pd/Ti10HMS	6	n.d. ^a

^a n.d. = not detectable.

2p_{3/2} and the O 1s binding energies are compiled along with the XPS-derived atomic ratios Ti/Si and Pd/(Ti + Si). The palladium 3d photoelectron spectra are characterized by the Pd 3d_{5/2} binding energy of 337.2 eV ± 0.2 eV. The value is typical of Pd⁴⁺ as in PdO₂.

Table 4
XPS binding energies and XPS-derived atomic ratios of the fresh catalysts.

Sample	Pd 3d _{5/2} (eV)	Ti 2p _{3/2} (eV)	O 1s ^a (eV)	Ti/Si ^b	Pd/(Ti + Si)
Pd/HMS	337.4		533.6		0.02
Pd/Ti5HMS	337.3	460.5	533.4 (97%) 530.6 (3%)	0.02 (0.04)	0.02
Pd/Ti10HMS	337.4	460.3	533.4 (94%) 530.9 (6%)	0.04 (0.08)	0.02
Pd/SBA	337.2		533.4		0.02
Pd/Ti5SBA-15	337.0	459.3	533.5 (90%) 530.6 (10%)	0.06(0.04)	0.02
Pd/Ti10SBA-15	337.0	459.4	533.5 (85%) 530.8 (15%)	0.08 (0.08)	0.02

^a The values in parentheses represent the atomic percentages of the oxygen chemical components.

^b The values in parentheses represent the nominal atomic ratios.

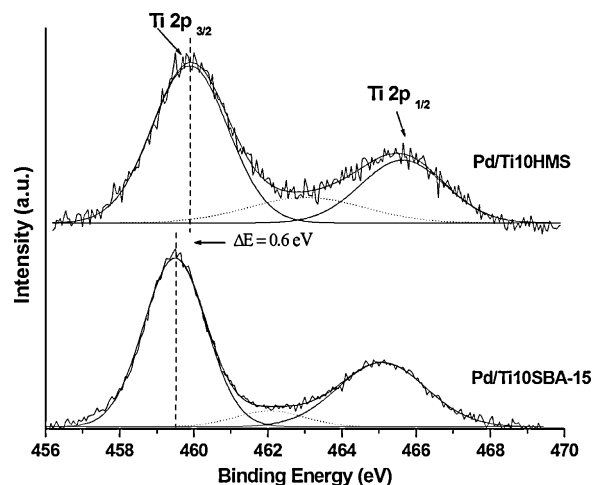


Fig. 5. Ti 2p photoelectron spectra of Pd catalysts supported on 10 wt% TiO₂ doped mesoporous silicas.

This oxide has been already reported for similar samples [19,34]. Its formation may be attained by oxygen incorporation into the PdO crystal lattice during calcination [34]. The Ti 2p spectra of the 10 wt% Ti(IV) doped catalysts are shown in Fig. 5. They are characterized by the two spin-orbit components, Ti 2p_{3/2} and Ti 2p_{1/2}, 5.7 eV apart. The third component at ≈462.5 eV ± 0.5 eV included in the fitted spectra is attributable to a contribution from the O 1s line excited by the Al Kβ line of the non-monochromatized radiation ($\Delta h\nu = 69.7$ eV) [31]. The binding energy of the Ti 2p_{3/2} in the pure TiO₂ oxides is 458.9 eV typical of a Ti⁴⁺ species [30,35]. In accord with a previous study [19], larger values of Ti 2p_{3/2} binding energy are observed for the titania incorporated silicas. The chemical shifts, with respect to the pure TiO₂ value, range from 1.6 eV in the HMS series to 0.5 eV for the SBA-15 series. Two contributions may be responsible for such significant shift, a “final state” and an “initial state effect”. As to the former effect, it generally accounts for the Ti 2p_{3/2} chemical shift when moving from Pd/Ti_xSi to Pd/TiO₂ [36]. It originates from the extra atomic relaxation energy [37] which is related to the polarizability of the oxide carrier. The less mobile the electrons are, as in SiO₂, the smaller is the relaxation energy and therefore the larger is the measured binding energy of the photoelectrons. This effect, related to the electrical property of the material, would produce analogous shift in the two types of mesoporous silica supported samples, therefore it could account for part of the total shift. The second effect, so called “initial state” effect, discussed already for a series of TiO₂-grafted SiO₂ [35,38] and responsible for a large shift between the two series of samples, may

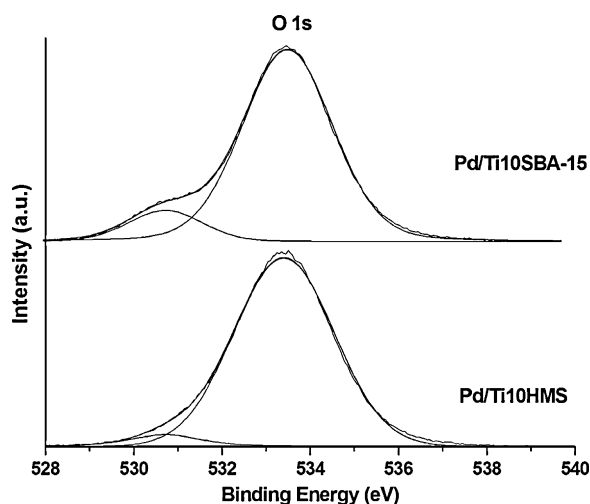


Fig. 6. O 1s photoelectron spectra of Pd catalysts supported on 10 wt% TiO₂ doped mesoporous silicas.

reflect the occurrence in the Ti(IV)-doped samples of an intimate association of TiO₂ and SiO₂, producing Ti–O–Si bonds where Ti⁴⁺ occupies tetrahedral coordination sites similar to Si in SiO₂ [39]. Since titanium is more electropositive than silicon, the increase of the positive charge on the titanium center of a Ti–O–Si bond as compared to Ti–O–Ti, would determine an increase of the Ti 2p binding energy. The larger shift observed in the HMS derived samples is in accord with the XRD results, suggesting a better titania dispersion in these samples as compared to the SBA-15 samples. The O 1s core level spectra of the mixed oxide supported catalysts are shown in Fig. 6 and the corresponding binding energies are listed in Table 4. The O 1s spectra were fitted with two components, a high binding energy one at $\approx 533.5 \text{ eV} \pm 0.1 \text{ eV}$ assigned to SiO₂ and a low binding energy feature at $530.7 \text{ eV} \pm 0.2 \text{ eV}$ closer to the value reported for TiO₂ [39]. It is worth noticing that the relative intensity of the low energy peak with respect to the high energy peak is significantly higher in the PdTi10SBA-15 as compared to the PdTi10HMS. This difference reflects larger surface amount of oxygen interacting with titanium and therefore larger amount of segregated TiO₂ at the surface of the PdTi10SBA-15 sample. As shown in Table 4, the experimental Ti/Si atomic ratio increases with increasing loadings of TiO₂, as expected from the nominal ratios given in parentheses. It is worth noticing the larger values of this ratio obtained for the titania doped SBA-15 samples as compared to the corresponding titania doped HMS samples. In accord with the oxygen results, this again indicates a preferential surface segregation of titanium in the SBA-15 supported catalysts. The Pd/(Ti + Si) atomic ratios listed in Table 4 are the same for all samples and, as predictable because of the adopted impregnation procedure, they are larger than the theoretical value of ~ 0.006 .

3.1.6. FT-IR

In Fig. 7 the FT-IR spectra in the OH stretching region of the activated HMS and SBA-15 samples are compared with the spectra of Pd-free and Pd-loaded 10% titania-doped mesoporous composites. The spectra of HMS and SBA-15 exhibit a sharp band at 3744 cm^{-1} , assigned to isolated Si–OH species [40]. The doping of HMS with 10 wt% TiO₂ results in a shift of the OH stretching vibration toward lower wavenumbers and appearance of a distinct shoulder at approximately 3690 cm^{-1} . The deposition of palladium causes disappearance of the absorptions at 3734 cm^{-1} and 3690 cm^{-1} and regeneration of the signal at 3744 cm^{-1} . This leads to the conclusion that the former two bands can be ascribed to titanol groups that serve as anchoring sites of the palladium species. The

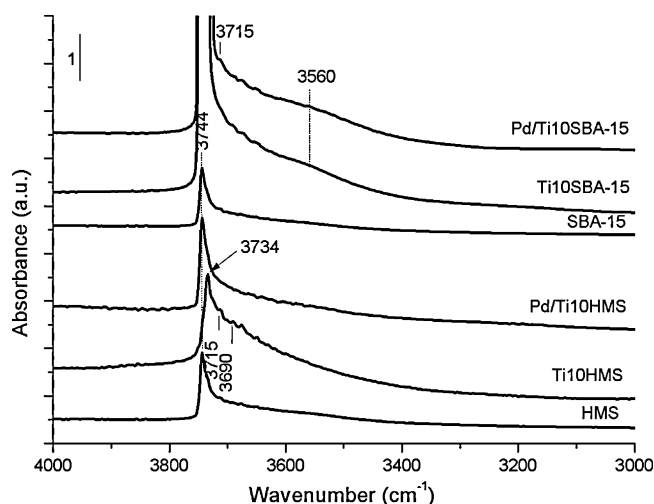


Fig. 7. FT-IR spectra of the samples in the OH stretching region.

Pd-free and Pd-loaded Ti10SBA-15 sample spectra display very strong absorption in the OH stretching region and the intensities of the corresponding bands are off-scale. This indicates that the OH groups induced by the modification of SBA-15 with titania are

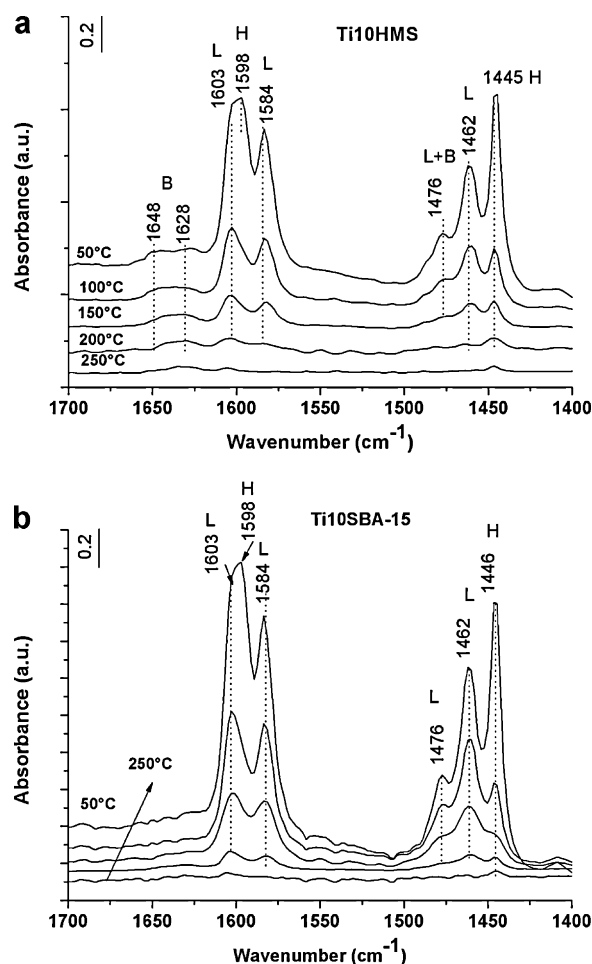


Fig. 8. (a) FT-IR spectra in the $1700\text{--}1400 \text{ cm}^{-1}$ region of the Ti10HMS sample recorded after adsorption of py at 25°C and subsequent desorption at various temperatures. (L, Lewis acidity; B, Brønsted acidity; and H, hydrogen bonded py) (b) FT-IR spectra in the $1700\text{--}1400 \text{ cm}^{-1}$ region of the Ti10SBA-15 sample recorded after adsorption of py at 25°C and subsequent desorption at various temperatures. (L, Lewis acidity; B, Brønsted acidity; and H, hydrogen bonded py.)

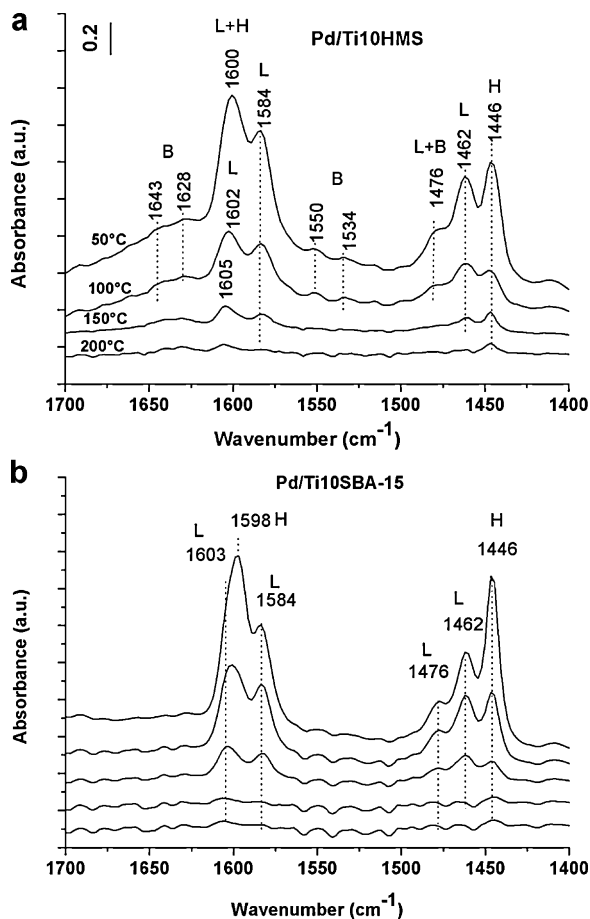


Fig. 9. (a) FT-IR spectra in the 1700–1400 cm^{-1} region of the Pd/Ti10HMS sample recorded after adsorption of py at 25 °C and subsequent desorption at various temperatures. (L, Lewis acidity; B, Brønsted acidity; and H, hydrogen bonded py) (b) FT-IR spectra in the 1700–1400 cm^{-1} region of the Pd/Ti10SBA-15 sample recorded after adsorption of py at 25 °C and subsequent desorption at various temperatures. (L, Lewis acidity; B, Brønsted acidity; and H, hydrogen bonded py.)

associated with the TiO_2 phase which is in agreement with the XRD and XPS results showing anatase crystallites at the surface of SBA-15. The shoulder at $\sim 3715 \text{ cm}^{-1}$, visible in the spectra of both Ti-containing supports is assigned to terminal Ti–OH groups [41]. The broad band at $\sim 3560 \text{ cm}^{-1}$ in the spectra of Ti10SBA-15 and Pd/Ti10SBA-15 samples is attributed to H-bonded silanol/titanol groups [40]. This absorption is absent in the spectra of Ti10HMS and Pd/Ti10HMS samples. The discrepancy is probably related to some structural differences between the two mesoporous silicas.

In order to discriminate the Brønsted and the Lewis acidity, the adsorption of pyridine (py) has been studied over the Ti-free and Ti-containing supports, and for the Pd catalysts. The spectra obtained upon room-temperature adsorption of the base followed by evacuation at various temperatures are shown in Figs. 8 and 9 for the Ti-doped supports and for the Pd catalysts respectively. All the spectra including those of the Ti-free supports (not shown in here) exhibited bands at 1598 and 1446 cm^{-1} due to non-acidic silanols and corresponding to py molecules weakly perturbed by H-bonding with the surface OH-groups [29,42–44]. In addition, a weak absorption at 1626 cm^{-1} from pyridinium ion on acidic Brønsted sites was observed also in both Ti-free supports [28,42–44]. However, the protonated base was weakly bound and disappeared during the evacuation at 100 °C. The doping of the HMS and SBA-15 supports by titania caused significant changes in the spectra of adsorbed py. As shown in Fig. 8, the bands at 1603 and 1462 cm^{-1} present only in the Ti-doped samples are attributed to the ν_{8a} and ν_{19b}

ring vibrations, respectively, of py molecules coordinated to strong Lewis acid sites, while the band at 1584 cm^{-1} reveals the presence of weak Lewis acid sites [28,42–44]. By evacuation at different temperatures, the intensities of the bands of py coordinated to Lewis acid sites decreases considerably. Small amount of coordinated py remains after degassing at 250 °C and pressure of $\sim 10^{-3}$ mbar. This indicates that the samples are characterized by a moderate Lewis acidity. The spectra of the Ti10HMS taken between 50 and 250 °C (Fig. 8a) contain a split broad band with maxima at 1648 and 1628 cm^{-1} which is attributed to the ν_{8a} and ν_{8b} vibrations of protonated py indicating the presence of Brønsted acid sites [28,42–44]. It should be noted that the band at around 1540 cm^{-1} that corresponds to the ν_{19b} vibration of py adsorbed on Brønsted acid sites is not observed. The reason for this could be the low concentration of surface hydroxyls with acidic protons. However, the absorptions at 1648 and 1628 cm^{-1} are clearly visible in all of the spectra taken in the 50–200 °C temperature range which confirm the presence of certain amount of weak Brønsted acidity in the Ti10HMS sample. Pyridinium ion vibrations at 1646 and 1628 cm^{-1} are not observed in the Ti10SBA-15 sample (Fig. 8b) indicating the absence of Brønsted acidity. Therefore for this material, the band at 1476 cm^{-1} (which can be assigned to py coordinated to both Brønsted and Lewis acid sites) is related only to Lewis acid sites. Several models have been proposed to explain the appearance of acid sites in a mixed oxide. The most accepted one is the model by Tanabe assuming that the extra charge generated by intimately mixing two oxides produces acidic sites of Brønsted or Lewis character depending on the sign of this charge [45,46]. Negative charge, balanced by association with protons, generates Brønsted sites whereas positive charge generates Lewis sites. Applying this model to the case of the mixed titania and silica oxide in the excess of silica, following the rules of the model, the charge excess at the titanium cation would be negative, therefore producing Brønsted acid sites. The effectiveness of the model implies a relationship between the molecular homogeneity and the acid site density. Then, the presence of Brønsted acid sites on the HMS samples may reflect a better Si/Ti structural homogeneity. The result would be in accord with the absence of anatase phase in the XRD patterns and also with the larger Ti 2p chemical shift and the lower intensity of the low energy O 1s component observed in the XP spectra of the HMS samples.

The spectra of pyridine adsorbed on the Pd promoted samples are given in Fig. 9. The comparison with the spectra of Fig. 8 indicates that the incorporation of palladium into the supports lowers the amount of Lewis acid sites, especially in the Pd/Ti10SBA-15 sample. Moreover, the absorption band in the 1675–1620 cm^{-1} range of the spectrum of the Pd/Ti10HMS catalyst (Fig. 9a), assigned to pyridine coordinated to Brønsted acid sites, becomes broader and stronger than that of the support. This suggests that the promotion of Ti10HMS with Pd generates additional Brønsted acidity and as a result, the total surface acidity of the Pd-containing Ti10HMS is higher than that of the Pd-free sample.

In order to get preliminary mechanistic information on the oxidation of methane and look for the formation of intermediate species, in situ FT-IR experiments were performed. The spectra of the palladium catalysts, during 15 min of exposure to a gas mixture containing 15 mbar CH_4 and 85 mbar O_2 at the various temperatures, were collected. The spectra for the Pd/Ti10HMS and Pd/Ti10SBA-15 are shown in Fig. 10. The positive absorption in the 3690–2700 cm^{-1} range indicates that the amount of H-bonded hydroxyls has increased as a result of water formation. The bands at 1635–1627 and 1534–1545 cm^{-1} are attributed to adsorbed carbonate species most likely coordinated to Ti sites [15,43] which are the intermediates for producing CO_2 . In spite of the close similarity between the spectra of the two samples, it is worth noticing the larger intensity of the peaks related to the adsorbed water and adsorbed carbonates at 350 °C in the

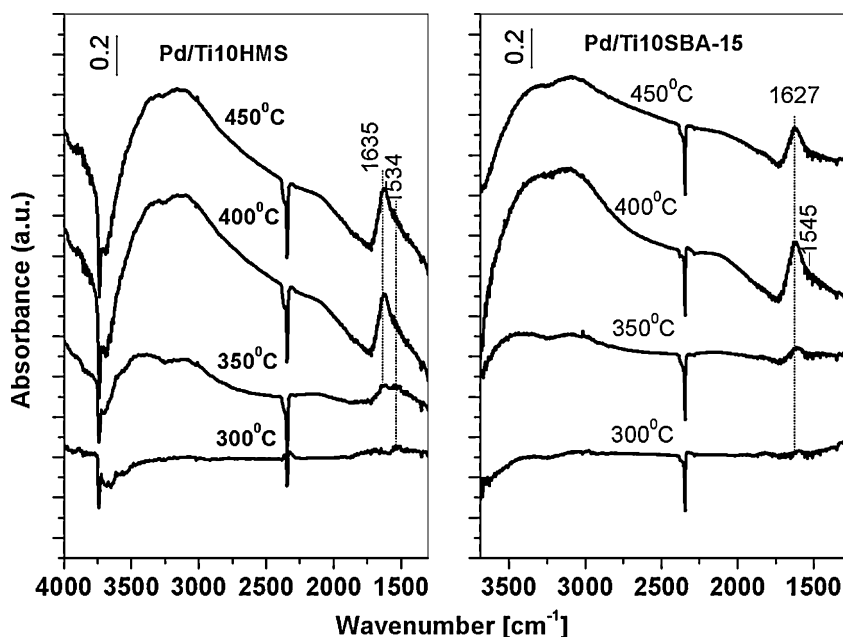


Fig. 10. FT-IR spectra recorded during the exposure of the Pd/10Ti-HMS and Pd/10Ti-SBA-15 catalysts to a mixture of 15 mbar CH_4 + 85 mbar O_2 at various temperatures.

spectrum of Pd/Ti10HMS sample as compared to the same peaks in the spectrum of Pd/Ti10SBA-15 sample. No other adsorption species related to the activated methane were detected. The presence of adsorbed formate species (HCOO^-), with typical bands at $3000\text{--}2700\text{ cm}^{-1}$ ($\nu\text{C-H}$ and combinations of fundamental frequencies) and at $1600\text{--}1550\text{ cm}^{-1}$ ($\nu_{\text{as}}\text{C-O}$), as intermediates of the reaction, could not be excluded [15,47]. The gas phase spectra (not shown here) indicated formation of CO_2 with peak observed at 2350 cm^{-1} .

3.2. Catalytic activity with SO_2 -free and SO_2 -containing reactant mixtures

In order to compare the catalytic performance of the catalysts, T_{50} values (corresponding to temperatures of 50% CH_4 conversion) of first and second runs performed sequentially using different conditions are listed in Table 5 along with the Arrhenius parameters. First cycles on the fresh samples were performed with pure reactant mixture and with SO_2 containing mixture. Then, in order to check for thermal instability and for possible residual contaminant effects, second runs were performed on samples aged upon exposure to the pure reactant mixture for 16 h at 600°C . Likewise, aiming to recover the catalyst activity after the first run in the presence of the poisoning SO_2 , a second cycle was performed using SO_2 -free reagents.

By inspection of Table 5, judging from the values of the T_{50} , the fresh Pd/HMS appears slightly more active as compared to the Pd/SBA-15. Quite interesting the long exposure to the reactants at 600°C , with some exceptions, determines an overall decrease of the T_{50} values which could be attributed to the removal of some residual organic precursors. As expected and in accord with previous results obtained with palladium supported on amorphous titania modified silica [19], the presence of 10 ppm of SO_2 in the reactant mixture deactivates the catalysts by causing a substantial increase of the T_{50} with respect to the cycles without SO_2 . Within these data it is worth noting the different behavior of the catalysts supported on silica HMS and silica SBA-15. The effect of the support modification by titania appears to be strongly related to the type of the support. In the case of SBA-15, an increase of titanium concentration improves the activity (lower T_{50}). On the contrary, in the

case of the HMS catalysts the addition of titanium in the support is detrimental since it produces an increase of the T_{50} . One possible explanation for the surprising behavior of the HMS catalyst could be the strong support acidity which hinders the preferential reaction of the SO_x with the support, beneficial for the palladium active sites. Considering the second cycle after the SO_2 exposure, the activity improves in all the samples, as already reported for palladium catalysts supported on high surface area silica [18,19]. The effect of titania on the catalytic performance is shown in Figs. 11 and 12, where selected plots of methane conversion as a function of temperature are given respectively for the HMS and the SBA-15 series of supported Pd catalysts. The curves refer to a first cycle with the SO_2 in the reactant mixture and to the subsequent cycle with the SO_2 free reactant mixture.

In order to get information on the active site variation, due to the oxide TiO_2 and/or to the SO_2 poisoning, the apparent activation energies were determined for the different catalytic runs. Neglecting the effect of small amounts of water formed in the process, the integral equation of a first order reaction with respect to methane and pseudo-zero order with respect to oxygen was used for the calculation of the reaction rate constants k [18,48]. Then, from

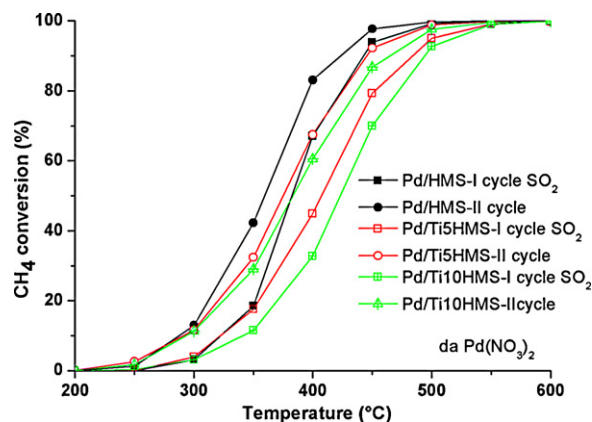


Fig. 11. Methane conversion as a function of temperature over HMS and Ti(IV) promoted HMS Pd catalysts for different cycles in different conditions.

Table 5Values of T_{50} (°C) and Arrhenius parameters^a, activation energy (E_{act}) and preexponential factor A (s^{-1}) of the catalysts, for the different reaction cycles.

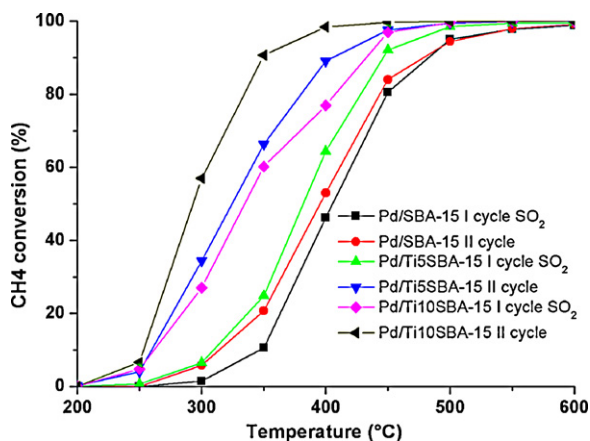
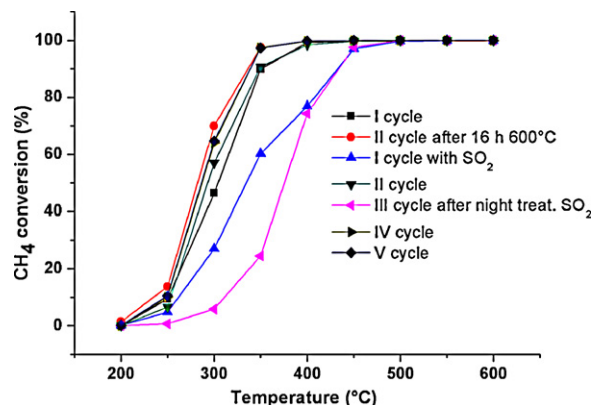
Sample	1st cycle			2nd cycle after 16 h at 600 °C			1st cycle with SO ₂			2nd cycle		
	T_{50} (°C)	E_{act} (kJ/mol)	ln A	T_{50} (°C)	E_{act} (kJ/mol)	ln A	T_{50} (°C)	E_{act} (kJ/mol)	ln A	T_{50} (°C)	E_{act} (kJ/mol)	ln A
Pd/SBA-15	341	77	17	346	71	16	405	125	25	395	85	18
Pd/Ti5SBA-15	302	78	19	308	73	17	383	90	19	325	77	18
Pd/Ti10SBA-15	304	76	20	282	67	21	334	79	18	292	75	18
PdHMS	322	79	18	289	76	18	382	120	24	359	81	18
Pd/Ti5HMS	344	97	21	334	69	16	407	85	18	375	72	16
PdTi10HMS ^b	n.a.			n.a.			422	81	16	383	73	14

^a E_{act} and A are calculated from the Arrhenius plot in the temperature range 250–350 °C.^b n.a. indicates that the tests for this sample were not performed.

the Arrhenius plot of $\ln(k)$ versus $1/T$, in the temperature range of 250–350 °C corresponding to conversions ranging between 10% and 80%, the activation energies E_{act} and the pre-exponential factors A of the Arrhenius equation, $k = A \exp(-E_{act}/RT)$, were calculated and listed also in Table 5. With some exceptions, the values of the activation energies are between 70 and 85 kJ/mol, which are close to those reported previously for similar catalysts for the same temperature range [19]. A careful inspection of the table gives interesting hints about the structural changes upon the chemical reactions. Although most of the variations are within the experimental error ($\pm 10\%$), some systematic changes are envisaged which can be related to structural modification due to the reaction. After a thermal treatment at 600 °C for 16 h, a lower value of the activation energy is observed, corresponding in some cases to an enhancement of the activity (lower T_{50}). As reported before, the presence of SO₂ in the reactant mixture causes an increase of the activation energy, quite remarkable in the samples without TiO₂ in the support [18]. Then, for all the samples, the subsequent cycle after the SO₂ exposure is characterized by lower activation energy and by a partial recovery of the activity. The activity is completely regained in the case of the Ti promoted SBA supported catalysts, but only partially recovered in the pure SBA-15, HMS and Ti-doped HMS supported catalysts. The increase of the activation energy during the run in the presence of SO₂ confirmed the earlier idea that sulfur deactivation was related to the formation of a composite species of lower activity, like PdO–SO₃, quite labile and easily decomposing at temperature ≥ 450 °C [18,19].

3.3. Stability, deactivation and structural changes of Pd/Ti10SBA-15

The most interesting sample, the PdTi10SBA-15 exhibiting the lowest T_{50} during the cycle with SO₂ and during the second cycles,

**Fig. 12.** Methane conversion as a function of temperature over SBA-15 and Ti(IV) promoted SBA-15 Pd catalysts for different cycles in different conditions.**Fig. 13.** CH₄ conversion as a function of temperature over Pd/Ti10SBA-15 for different cycles in different conditions.

was selected for a series of consecutive cycles in order to test its stability, deactivation and activity recovery. Particularly, after a first cycle with the SO₂ containing reagents and a second cycle with SO₂-free reagents, the sample underwent an overnight treatment in flowing 10 vol. ppm of SO₂ in He at 350 °C at a flow rate of 50 ml/min. After this treatment three more cycles with the pure reagents were performed. All the related conversion curves are given in Fig. 13 including also the two curves (I cycle SO₂ and II cycle) given already in Fig. 2. The corresponding values of T_{50} and Arrhenius parameters are listed in Table 6. For the sake of clarity some of the values are duplicated from Table 5. A remarkable increase of the T_{50} is observed after the night treatment with SO₂. At the same time, an increase of the activation energy up to 114 kJ/mol is obtained. In the following 4th and 5th cycles, the activity is completely recovered. It is remarkable that the final values of the activation energies (95–94 kJ/mol), although decreased with respect to the value obtained after the severe deactivation, do not reach the lowest value of 67 kJ/mol obtained for the second cycle. The significant difference, well above the experimental error, could reflect some structural changes of the active site and, as long as the

Table 6Values of T_{50} (°C) and Arrhenius parameters^a, activation energy (E_{act}) and preexponential factor A (s^{-1}) of the Pd/Ti10SBA-15 catalyst for the different reaction cycles.

Reaction cycle	T_{50} (°C)	E_{act} (kJ/mol)	ln A
1st cycle	304	76	20
2nd cycle after 16 h exposure to the reaction mixture at 600 °C	282	67	21
1st cycle SO ₂	334	79	18
2nd cycle SO ₂ -free	292	75	18
3rd cycle after overnight SO ₂ treat.	375	114	23
4th cycle	287	95	22
5th cycle	286	94	22

^a E_{act} and A are calculated from the Arrhenius plot in the temperature range 250–350 °C.

Table 7
XRD derived PdO and TiO₂ particle diameters and XP Pd 3d_{5/2} binding energy and Ti/Si and Pd/(Ti + Si) atomic ratios in spent catalysts.

Sample	d _{PdO} (nm)	d _{TiO₂} (nm)	Pd 3d _{5/2} (eV)	Ti/Si	Pd/(Ti + Si)
PdTi10SBA-15 after 5th cycle including SO ₂ night treat.	18	7	337.0	0.08	0.005
PdTi10SBA-15 after 4 days reaction at 600 °C	16	8	337.3	0.07	0.005

final activity is concerned, is well compensated by an increase of the pre-exponential factor. On the same sample but on a different batch a stability test was performed by running a catalytic test after exposing the sample to the pure reagent mixture for 4 days at 600 °C. As revealed by the conversion curve (not given in here), matching exactly the curve of the second cycle, (Table 6 second row data) no change in the catalytic performance occurred.

In order to check for structural modification, the two aged samples were analysed by SAXS, XRD and XPS techniques. According to the SAXS patterns (not shown here) the SBA-15 mesoporous structure of the aged catalysts was maintained. The XRD patterns of the fresh sample and the corresponding patterns of the sample after 5 cycles including the SO₂ overnight treatment (refer to Table 6) and the sample after the long run of 4 days at 600 °C are compared in Fig. 14. The patterns contain the TiO₂ anatase peaks and the PdO related peaks. The calculated TiO₂ and PdO particles size are given in Table 7. It is worth noticing that whereas the TiO₂ particles maintain the same size, the PdO particle size drastically increases after the long run with the pure reagent mixtures and also after five cycles including the overnight exposure to the SO₂ at 350 °C. The increase of the PdO particle size upon similar sequence of reaction cycles was also observed recently with a palladium catalyst supported on amorphous Ti10SiO₂ [20]. It should be pointed out that the XRD technique identifies the larger particles, whereas small particle sizes, below the limit of 3 nm, are not detected. Then, in order to ultimately confirm the decrease of palladium dispersion, XPS analyses of the samples, after several cycles including the overnight SO₂ exposure and after the stability tests, were performed. The XPS results of the spent samples are listed in Table 7. As compared to the corresponding values of the fresh sample, as given in Table 4, no significant changes in the palladium binding energy and in the Ti/Si atomic ratio are observed. However the smaller values of the Pd/(Ti + Si) atomic ratios as compared to the fresh sample are in accord with the enlargement of the PdO particle size revealed by the XRD. It is worth noticing that in spite of this serious palladium sintering the catalytic activity of the catalyst was maintained. A recent study on palladium supported on silica SBA-15, modified by ceria and by zirconia, reported a loss of activity, upon a severe deactivation test, for catalysts show-

ing good PdO particle stability [13]. The conclusion of the work was that the loss of catalyst activity during reaction was not necessarily related to the sintering of the active sites but rather to the variation of the oxygen storage capacity and oxygen mobility strictly related to the support properties. It is accepted that Pd-catalysed combustion of methane occurs through a redox or Mars van Krevelen mechanism [17,49]. Accordingly, during this reaction PdO is locally reduced to Pd by methane, producing H₂O and CO₂, and then Pd is reoxidised by oxygen. Although the active species is considered PdO, it is widely recognized that metallic Pd plays the important role in decomposing and activating the methane molecule [3,15,50]. Therefore, the efficiency of the all process is related to the redox properties of the catalyst and to the oxygen mobility [17]. In the present case, the maintenance of the activity, in spite of the significant palladium oxide sintering, could be attributed to the good interaction between surface titania and silica. Such interaction, as reported in previous papers, favors the formation of Ti–O–Si linkages with an increase of the oxidizing potential of the Ti(IV) cations [38,51]. The increase of this potential would enhance the oxygen mobility at the interface between the Ti–O–Si units and the palladium particles [38,49]. On this account, the stability of the Pd/Ti10SBA-15 catalyst, observed after a long lasting reaction at 600 °C and after several cycles including the overnight SO₂ exposure, is likely related to the oxygen mobility which allows the reoxidation of the Pd to PdO. In the presence of a support metal–interaction, the increase of the PdO particle size after the long reaction is not detrimental. Indeed, an inverse particle size structure sensitivity of the palladium catalysed methane combustion was claimed, related to the high stability of the small PdO particles interacting with the support and not being easily reduced [13,50].

4. Conclusion

The effect of the addition of titania to different mesoporous silica oxides on the methane oxidation activity of supported palladium was found to depend on the type of mesostructured material. The addition of 10 wt% of TiO₂ to the silica SBA-15, improved the catalytic performance of the supported palladium catalysts, in terms of better activity and better sulfur tolerance as compared to palladium over pure SBA-15 support. This result confirmed the positive effect played by titania, acting as SO₂ scavenger, on Pd catalysts supported on amorphous silica [19]. Opposite behavior was observed with the HMS samples. In this case addition of TiO₂ produced poorer catalysts in terms of lower activity and lower SO₂ tolerance. According to the structural and morphological analyses, the two series of catalysts had similar palladium dispersion and similar surface area but different TiO₂ distribution. In the case of the HMS, Ti(IV) ions were homogeneously distributed into the silica framework, whereas a mixture of framework Ti(IV) and surface segregated TiO₂ anatase particles was present in the SBA-15. Due to the more uniform distribution of Ti(IV) into the silica matrix, a substantial increase of the total acidity, in particular of the Brønsted type, developed in the Ti_xHMS support as compared to the SBA-15. Moreover, through the in situ FT-IR, more adsorbed water and carbonate species were observed on the Pd/Ti10HMS as compared to the Pd/Ti10SBA-15. On the bases of these evidences, the formation of a stronger acidity and the presence of Brønsted sites were responsible for the negative effect of the titania on the methane oxidation activity of the

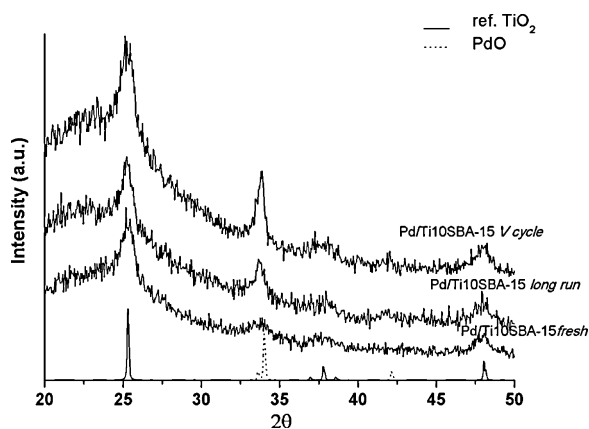


Fig. 14. XRD patterns of PdTi10SBA-15 catalyst as fresh, after 5th cycle including overnight SO₂ treatment at 350 °C and after four days of catalytic reaction at 600 °C (long run).

HMS supported Pd catalysts. Indeed, the stronger water adsorption over the acidic support would inhibit the catalytic methane oxidation favoring formation of the less active Pd(OH)₂ and also blocking the active sites through surface diffusion. The large amount of adsorbed carbonate species, detected in the Pd/Ti10HMS catalyst by the in situ FTIR analyses at 350 °C, could have also contributed to the deactivation of the catalysts. Furthermore, the creation of the stronger acidity, by hindering the preferential reaction of the SO_x with the support, nullified the scavenger action of the titania.

Acknowledgements

This research has been performed in the framework of the D36/003/06 COST program and a NATO grant ESP.CLG. No. 984160.

References

- [1] P. Gelin, M. Primet, *Appl. Catal. B* 39 (2002) 1–37.
- [2] F. Arosio, S. Colussi, G. Groppi, A. Trovarelli, *Catal. Today* 117 (2006) 569–576.
- [3] T.V. Choudhary, S. Banerjee, V.R. Choudary, *Appl. Catal. A* 234 (2002) 1–23.
- [4] R. Burch, M.J. Hayes, *J. Mol. Catal. A* 100 (1995) 13–33.
- [5] Y.-x. Pan, C.-j. Liu, P. Shi, *Appl. Surf. Sci.* 254 (2008) 5587–5593.
- [6] L.F. Liotta, G. Di Carlo, G. Pantaleo, A.M. Venezia, G. Deganello, *Appl. Catal. B* 66 (2006) 217–227.
- [7] N. Bahlawane, *Appl. Catal. B* 67 (2006) 168–176.
- [8] Z. Gao, R. Wang, *Appl. Catal. B* 98 (2010) 147–153.
- [9] E. Tzimpilis, N. Moschoudis, M. Stoukides, P. Bekiaroglou, *Appl. Catal. B* 87 (2009) 9–17.
- [10] Z. Jiang, Z. Hao, J. Su, T. Xiao, P.P. Edwards, *Chem. Commun.* 22 (2009) 3225–3227.
- [11] J.K. Lambert, M.S. Kazi, R. Farrauto, *J. Appl. Catal.* 14 (1997) 211–223.
- [12] H. Yoshida, T. Nakajima, Y. Yazawa, T. Hattori, *Appl. Catal. B* 71 (2007) 70–79.
- [13] F. Yin, S. Ji, P. Wu, F. Zhao, C. Li, *J. Catal.* 257 (2008) 108–116.
- [14] K. Persson, K. Jansson, S.G. Järas, *J. Catal.* 245 (2007) 401–414.
- [15] M. Schmal, M.M.V.M. Souza, V.V. Alegre, M.A. Pereira da Silva, D.V. Cesar, C.A.C. Perez, *Catal. Today* 118 (2006) 392–401.
- [16] N.M. Kinnunen, M. Suvanto, M.A. Moreno, A. Savimaki, K. Kallinen, T.-J.J. Kinnunen, T.A. Pakkanen, *Appl. Catal. A* 370 (2009) 78–87.
- [17] K. Fujimoto, F.H. Ribeiro, M.A. Borja, E. Iglesia, *J. Catal.* 179 (1998) 431–442.
- [18] A.M. Venezia, R. Murania, G. Pantaleo, G. Deganello, *J. Catal.* 251 (2007) 94–102.
- [19] A.M. Venezia, G. Di Carlo, G. Pantaleo, L.F. Liotta, G. Melaet, N. Kruse, *Appl. Catal. B* 88 (2009) 430–437.
- [20] G. Di Carlo, G. Melaet, N. Kruse, L.F. Liotta, G. Pantaleo, A.M. Venezia, *Chem. Commun.* 46 (2010) 6317–6319.
- [21] N. Marin-Astorga, G. Pecchi, T.J. Pinnavaia, G. Alvez-Manoli, P. Reyes, *J. Mol. Catal. A* 247 (2006) 145–152.
- [22] P.T. Tanev, M. Chibwe, T.J. Pinnavaia, *Nature* 368 (1994) 321–323.
- [23] D. Zhao, J. Feng, Q. Huo, N. Melosh, G.H. Fredrickson, B.F. Chmelka, G.D. Stucky, *Science* 279 (1998) 548–552.
- [24] S.J. Gregg, K.S. Sing, *Adsorption, Surface Area and Porosity*, second ed., Academic Press, San Diego, 1982.
- [25] JCPDS Powder Diffraction File Int. Centre for Diffraction Data, Swarthmore, 1989, File No. 42-1467.
- [26] H.P. Klug, *X-ray Diffraction Procedure for Polycrystalline and Amorphous Materials*, Wiley, New York, 1954.
- [27] V. La Parola, B. Dragoi, A. Ungureanu, E. Dumitriu, A.M. Venezia, *Appl. Catal. A* 386 (2010) 43–50.
- [28] A. Tuel, *Micropor. Mesopor. Mater.* 27 (1999) 151–169.
- [29] W. Zhang, M. Fröla, J. Wang, P.T. Tanev, J. Wong, T.J. Pinnavaia, *J. Am. Chem. Soc.* 118 (1996) 9164–9171.
- [30] T.A. Zepeda, *Appl. Catal. A* 347 (2008) 148–161.
- [31] N.N. Trukhan, V.N. Romanikov, A.N. Shmakov, M.P. Vanina, E.A. Paukshtis, V.I. Bukhtiyarov, V.V. Kriventsov, I.Yu. Danilov, O.A. Kholdeeva, *Micropor. Mesopor. Mater.* 59 (2003) 73–84.
- [32] W. Li, S.J. Huang, S.B. Liu, M.O. Coppens, *Langmuir* 21 (2005) 2078–2085.
- [33] Z. Luan, E.M. Maes, P.A.W. Van der Heide, D. Zhao, R.S. Czernuszewics, L. Kevan, *Chem. Mater.* 11 (1999) 3680–3686.
- [34] Y. Bi, G. Lu, *Appl. Catal. B* 41 (2003) 279–286.
- [35] E. Santacesaria, M. Cozzolino, M. Di Serio, A.M. Venezia, R. Tessier, *Appl. Catal. A* 270 (2004) 177–192.
- [36] G. Lassaletta, A. Fernandez, J.P. Espinós, A.R. Gonzalez-Elipe, *J. Phys. Chem.* 99 (1995) 1484–1490.
- [37] C.D. Wagner, *Faraday Discuss. Chem. Soc.* 60 (1975) 291–300.
- [38] A.M. Venezia, F.L. Liotta, G. Pantaleo, A. Beck, a. Horvath, O. Geszti, A. Kocsyony, L. Gucci, *Appl. Catal. A* 310 (2006) 114–121.
- [39] R. Castillo, B. Koch, P. Ruiz, B. Delmon, *J. Catal.* 161 (1996) 524–529.
- [40] N.N. Trukhan, A.A. Panchenko, E. Roduner, M.S. Mel'gunov, O.A. Kholdeeva, J. Mrowiec-Białoń, A.B. Jarzębski, *Langmuir* 21 (2005) 10545–10554.
- [41] M.I. Zaki, M.A. Hasan, F.A. Al-Sagheer, L. Pasupulety, *Colloids Surf. A* 190 (2001) 261–274.
- [42] M. Hunger, U. Schenk, M. Breuninger, R. Gläser, J. Weitkamp, *Micropor. Mesopor. Mater.* 27 (1999) 261–271.
- [43] G. Busca, *Catal. Today* 41 (1998) 191–206.
- [44] R.S. Araujo, D.A.S. Maia, D.C.S. Azevedo, C.L. Cavalcante Jr., E. Rodriguez-Castellon, A. Jimenez-Lopez, *Appl. Surf. Sci.* 255 (2009) 6205–6209.
- [45] K. Tanabe, T. Sumiyoshi, K. Shibita, T. Kiyoura, J. Kitagawa, *Bull. Chem. Soc. Jpn.* 47 (5) (1974) 1064.
- [46] J.B. Miller, E.I. Ko, *Catal. Today* 35 (1997) 269–292.
- [47] G. Busca, V. Lorenzelli, *Mater. Chem.* 7 (1982) 89–126.
- [48] L.J. Hoyos, H. Praliad, M. Primet, *Appl. Catal. A* 98 (1993) 125–138.
- [49] C.A. Muller, M. Maciejewski, R.A. Koeppel, A. Baiker, *J. Catal.* 166 (1997) 36–43.
- [50] S.C. Su, J.N. Carstens, A.T. Bell, *J. Catal.* 176 (1998) 125–135.
- [51] X. Gao, I.E. Wachs, *Catal. Today* 51 (1999) 233–254.